Materials Research Bulletin 102 (2018) 391–398

Contents lists available at ScienceDirect

Materials Research Bulletin

journal homepage: www.elsevier.com/locate/matresbu

Activated biomass carbon made from bamboo as electrode material for supercapacitors

Guoxiong Zhang, Yuemei Chen, Yigang Chen*, Haibo Guo

Department of Electronic Information Materials, School of Materials Science and Engineering, Shanghai University, Shanghai 200444, China

ARTICLE INFO

Keywords:
Bamboo
Activation temperature
Supercapacitor
Energy storage

ABSTRACT

Activated biomass carbons (ABC) produced from bamboo by carbonization and activation have high specific surface areas and mesoporous structures. The specific surface area, total pore volume, and average pore size of the activated biomass carbon are controlled by adjusting the activation temperature from 700 to 1000 °C. The carbon materials activated at 900 °C have an optimal mesoporous structure with a high specific surface area (2221.1 $m^2 g^{-1}$), the highest capacitance (293 F g^{-1} at 0.5 A g^{-1} in 3 M KOH aqueous electrolyte) and excellent rate capability (193.8 F g^{-1} at 20 A g^{-1}). Symmetric supercapacitors made of the optimal electrodes exhibit a high energy density of 10.9 Wh kg^{-1} (18.2 Wh L^{-1}) at a power density of 63 W kg^{-1} (105 W L^{-1}) and outstanding capacitance retention of 91.8% over 10,000 cycles. The high electrochemical performance of the mesoporous ABCs show that they are highly promising for energy-storage applications with further optimization.

1. Introduction

The fast development of economy growth and the sharp increase of population have resulted a grim complexion that global environmental deterioration and depletion of energy resources [1]. Environment-friendly energy supply is one of the most important concerns for our lives [2]. It is essential to create new generations of energy storage and conversion devices. Considerable amount of work has been devoted to the development of advanced energy-storage devices and management systems for addressing ever-increasing energy demand and environmental issues [3]. Supercapacitors possessing high specific power and energy densities, fast charge/discharge rates, excellent rate capability, and long cycle life, have drawed much attention as one of the most promising energy-storage devices [3–5].

In the last decade, activated carbon materials have drawn much attention as electrodes of supercapacitors due to their large surface areas, controllable pore size, and high chemical stability. Unfortunately, their poor conductivity and single micropore structure strongle affect their capacitive performance because their inner pores are difficult to be fully accessed by electrolyte, resulting in a low capacitance (< 200 F g^{-1}) and a low energy density(5–8 W h kg^{-1}) [6,7]. Ion diffusion and charge propagation would be facilitated in porous carbon by effective combination of micropores and mesopores [8,9]. Moreover, improving conductivity of carbon materials also benefits rapid transport of ions in the electrodes. Therefore, it is a critical need to find advanced carbon-based material with high conductivity and proper pore size.

Recently, several new carbon-based materials have been developed with improved conductivity and proper pore size. Among them biomass-carbon materials are of special interest as they are sustainable and renewable, and can exhibit outstanding electrochemical performance due to their natural porous structures (high surface area) and high conductivity [10,11]. For instance, Kumagai et al. [12] used a mixture of rice husk (RH) and beet sugar as raw materials to produce micro- and meso-porous RH-derived activated carbons (ACs) with a specific surface area of approximately 1357 $m^2 g^{-1}$, showing a specific capacitance of 106 F g^{-1} in a 1M H_2SO_4 aqueous electrolyte at 5 mV s^{-1}. Activated carbon has been synthesized from cow dung with a chemical activation method by Bhattacharjya et al. [13], and showed a high surface area (1510 $m^2 g^{-1}$) and specific capacitance (117 F g^{-1} at 1 A g^{-1}). Jin et al. [14] obtained activated carbon from corn stover by microwave and slow pyrolysis, and the specific capacitance reached 245.9 F g^{-1} at 0.1 A g^{-1}. The capacitances of the activated carbons mentioned above are much lower than the activated carbon derived from olive pits by Redondo et al. [15], who reported an ultrahigh specific capacitance of 260 F g^{-1} at 0.5 A g^{-1} in KOH aqueous electrolyte. Hence, it could be concluded that the electrochemical performance of ACs have a strong dependence on the microstructure and specific surface area [16]. In the south of China, bamboo has been widely used as building material and medical material due to its low cost and abundance. Furthermore, as a kind of renewable biomass material, bamboo has a porous network structure, which is advantageous in electrochemical processes for high-

* Corresponding author.
E-mail address: yigangchen@shu.edu.cn (Y. Chen).

https://doi.org/10.1016/j.materresbull.2018.03.006
Received 12 June 2017; Received in revised form 2 March 2018; Accepted 3 March 2018
Available online 05 March 2018
0025-5408/

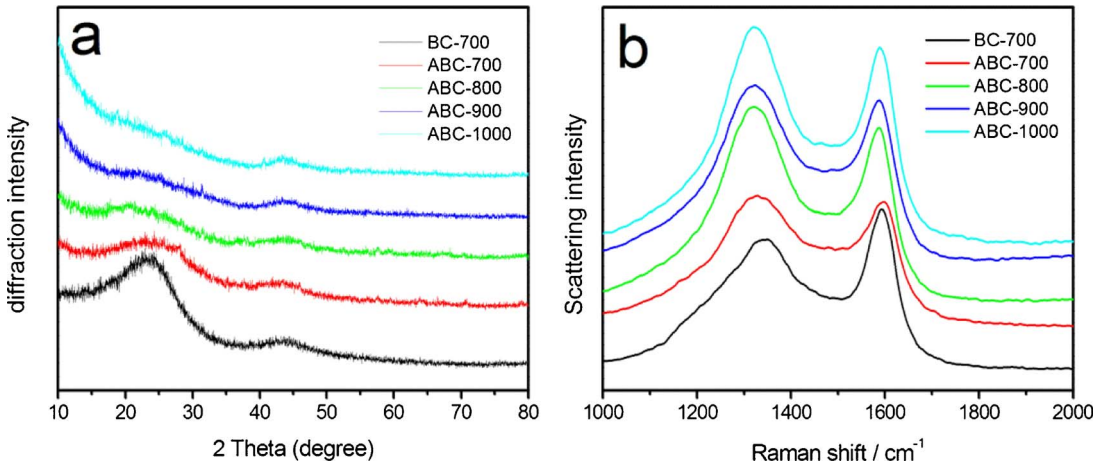

Fig. 1. XRD pattern (a) and Raman spectra (b) of activated carbons and their precursor.

Table 1
The specific surface areas, total pore volumes, and average pore sizes of activated carbons and their precursor.

Sample	Specific Surface areas ($m^2 g^{-1}$)	Total pore volumes ($cm^3 g^{-1}$)	Average pore sizes (nm)
BC-700	674.3	0.382	3.044
ABC-700	1028.6	0.599	2.384
ABC-800	2133.3	1.273	2.428
ABC-900	2221.1	1.238	2.257
ABC-1000	2715.1	1.509	2.282

performance electrical double-layer capacitors [17].

Herein, activated biomass carbon has been successfully prepared from bamboo by a simple method involving carbonization and KOH activation processes. To optimize the microstructures of the activated biomass carbon, the most important process parameter, activation temperature, is varied from 700 °C to 1000 °C, and the resultant materials have been assembled in symmetric supercapacitors and tested for electrochemical performance. Our results show that the activated biomass carbon has a mesoporous structure and a large surface area providing active sites to enhance ion transport between electrolyte and the carbon, resulting in outstanding electrochemical properties. The results indicate that the activated biomass carbons as electrode materials would be promising for supercapacitor applications.

2. Experimental

2.1. Preparation of activated biomass carbon (ABC)

Carbonization process: Biomass collected from a farm were cleaned and air-dried. Biomass pieces from the bamboos were calcined under N_2 flow at 200 °C for 1 h to decompose the organics, then heated at 700 °C for 3 h for carbonization. The carbonized materials were washed with HF (20%) to remove SiO_2, and subsequently with HCl (40%) to remove $CaCO_3$. Finally, the materials were washed with deionized water until the pH of the wash water reached 7. The carbonized materials are denoted as BC-700.

KOH activation process: The carbonized materials and KOH were mixed in the weight ratio of 1:3. The mixture were placed in corundum crucible and activated at 700, 800, 900, and 1000 °C, respectively, for 3 h under N_2 flow. After cooling down to the room temperature, the activated carbon materials were washed with deionized water until the pH of the wash water reached 7. The sample were then dried at 75 °C for 6 h. The activated biomass carbon are denoted as ABC-700, ABC-800, ABC-900, and ABC-1000, respectively.

2.2. Characterization techniques

The crystal structures of the activated biomass carbon materials were examined by powder X-ray diffraction with Cu k_α radiation (λ = 0.154056 nm). Raman spectra were recorded on a Raman microscope in the range of 1000–2000 cm^{-1}. Scanning electron microscopy (SEM) images were captured on a Quanta FEG-250 scanning electron microscopy. The specific surface area and pore size distribution was calculated using a mode 3H-2000PS2 instrument using nitrogen as the adsorbate at 77 K.

2.3. Electrocatalytic evaluation

Electrochemical tests were performed using a three-electrode system at a CHI660E electrochemical workstation. A Hg/HgO electrodes, and a Pt plate were used as reference electrode and counter electrode, respectively. A Ni foam supporting a mixture that contains 80 wt% activated biomass carbon, 10 wt% acetylene black, and 10 wt% polytetrafluoroethylene (PTFE) was used as working electrode. The activated biomass carbon loaded on the Ni foam was approximately 6 mg cm^{-2}.

For electrocatalytic evaluation in a two-electrode setting, the electrode were prepared on circular nickel foams (Φ15 mm), which each contained 4–5 mg of active material. A symmetric supercapacitor was fabricated using a CR2016 shell, which encapsulated two pieces of Ni foam supporting the activated biomass carbons, and a porous non-woven cloth separator. Electrochemical impendence spectroscopy (EIS) was measured in the frequency range from 10^5 to 10^{-2} Hz. The LAND battery program-control test system was used to test the cycling performances of the symmetric supercapacitors.

3. Results and discussion

The XRD pattern of the activated biomass carbons and their precursor are shown in Fig. 1(a). No sharp peaks are visible in Fig. 1(a), indicating that the as-synthesized samples are in an amorphous [18]. The diffraction peaks at 23.4° and 43.7° are characteristic of amorphous carbon. Especially the characteristic peak at 43.7° is associated with

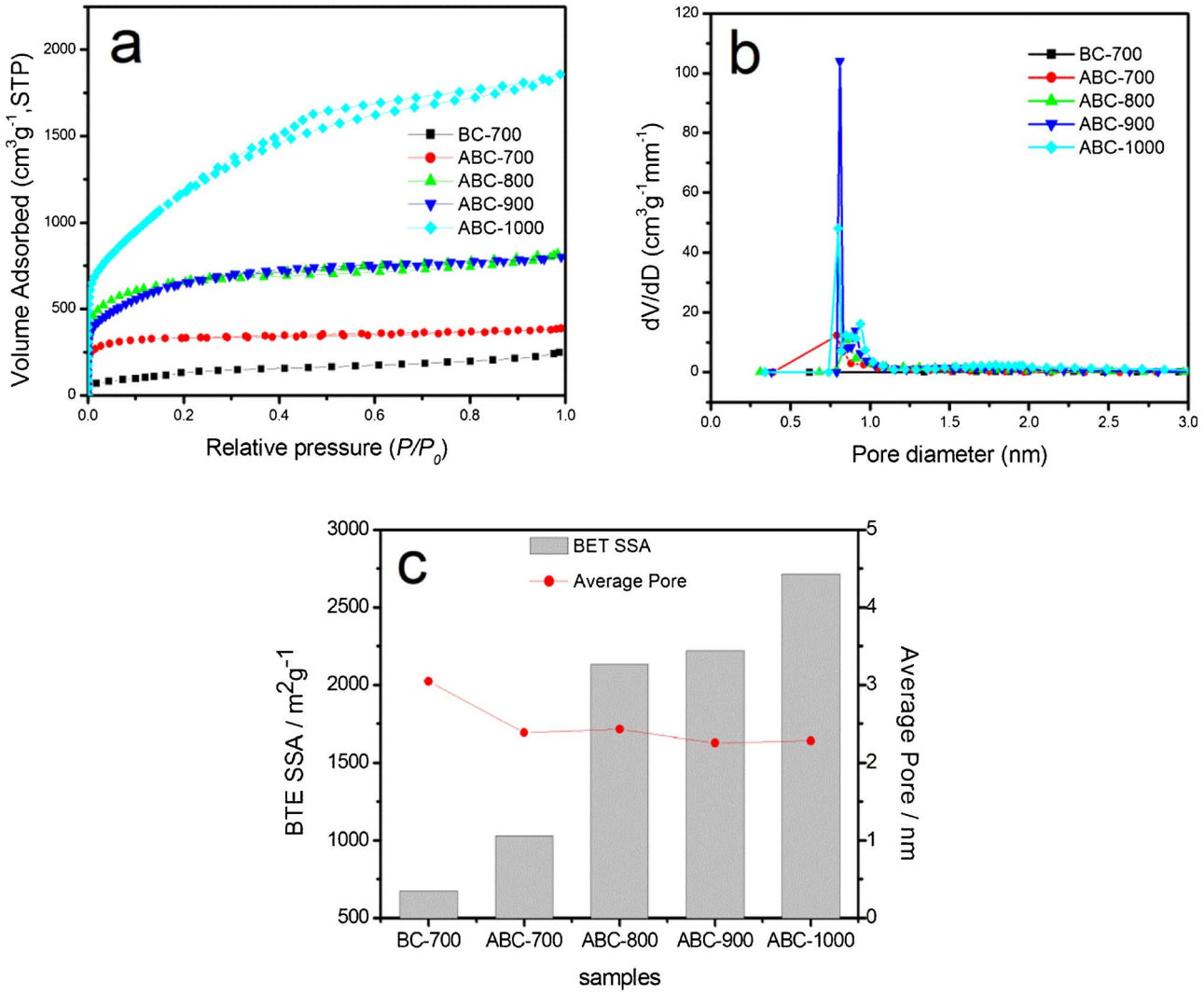

Fig. 2. N_2 sorption and porosity characteristics (a) and Pore size distributions (b) of different carbon materials. (c) BET specific surface areas and average pore sizes as functions of activation temperature.

electrical conductivity of carbon materials [19]. With increasing activation temperature from 700 to 1000 °C, the characteristic peak centered at 23.4° of the activated biomass carbons significantly decreases in intensity and broadens in width, indicating the orderliness in the atomic arrangement has been increasingly destroyed after the KOH activations [18].

The Raman spectra of the activated biomass carbons and their precursor are shown in Fig.1(b). The two characteristic peaks correspond to the disorder-induced bands (D bands, ~1350 cm^{-1}) and graphite bands (G bands, ~1590 cm^{-1}) of carbon, respectively. The D band reflects the defects and disorder in the samples, while the G band represents the ordered sp^2 carbon plane. The intensity ratio of D band and G band (I_D/I_G) is taken as a measure of disorder degree and graphization of carbon materials [20,21]. The I_D/I_G of BC-700, ABC-700, ABC-800, ABC-900, and ABC-1000 sample are 0.81, 1.05, 1.08, 1.14, and 1.16, respectively. With the increasing of activation temperature, the increase of the I_D/I_G ratio indicates that the extent of disorder in atomic arrangement.

The pore properties of the activated biomass carbons and their precursor are further analyzed from N_2 gas sorption spectra. The N_2 sorption and porosity characteristics and Pore size distributions of the activated carbons and their precursor are shown in Table 1 and Fig. 2. The activation temperature has a great influence on the porosity of the carbon materials. With the activation temperature increasing from 700 to 1000 °C, the specific surface area and total pore volume of the carbon materials increase by about two folds, and the average pore size decreases from 3.044 nm to 2.282 nm, indicating that the ABCs have mesoporous structure, and the carbon skeleton degrades at a high activation temperature. As shown in Fig. 2a, the adsorption/desorption curves of the $NiCo_2S_4$-SDS specimens belong to a type-IV isotherm with a H3 hysteresis loop, indicating the presence of a mesoporous structure. It has been reported that a mesoporous structure with a high BET surface area of activated carbons provides more active sites than nanoporous or microporous structures, and this can also improve transport of ions and electrochemical properties [16].

Fig. 3 shows the morphologies and structures of different activated biomass carbons. The structures of the bamboo before and after calcination are shown in Fig. 3(a–b). The ordered porous structures of the bamboo are well destroyed after calcination at 700 °C. The SEM images of the bamboo activated by KOH are shown in Fig. 3(c–f). Regardless of

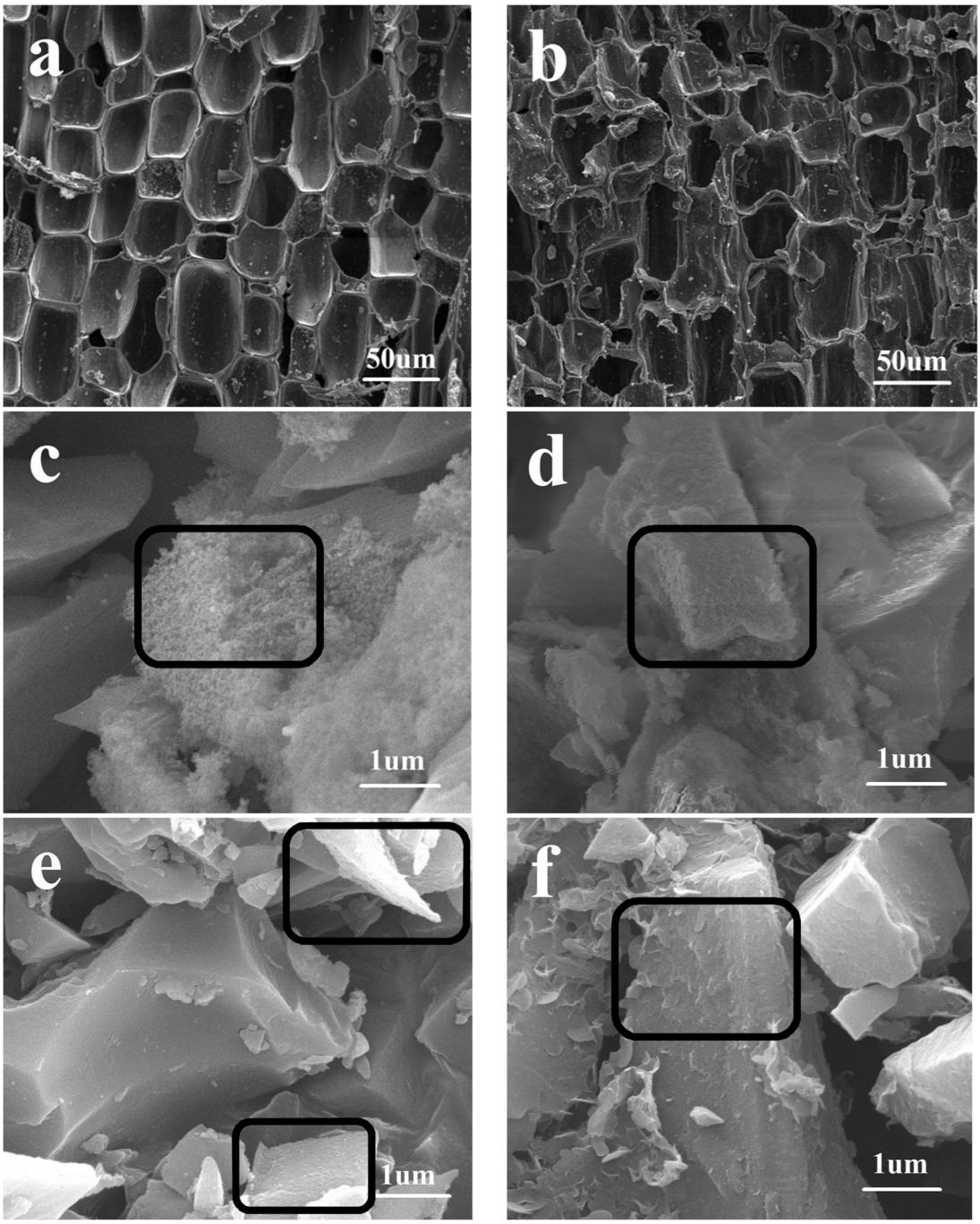

Fig. 3. SEM images of bamboo before calcination (a), after calcination (b). FESEM images of ABC-700 (c), ABC-800 (d), ABC-900 (e), and ABC-1000 (f) samples.

the activation temperature, all the carbon materials show irregular shapes and various sizes. Fig. 3(c) shows that abundant pores exist in the ABC-700 sample. With increasing activation temperature from 700 °C to 1000 °C, the mesoporous structure is gradually consolidated. However, the specific surface area and total pore volume of the carbon materials have an apparent improvement with the increasing of activation temperature from 700 °C to 1000 °C (Table 1), indicating that the structure of abundant pores still exists in the carbon materials, and that compactness of the porous structure increases with the activation temperature.

The detailed morphology and hollow structures were further confirmed by HRTEM, as shown in Fig. 4. Typical TEM images (Fig. 3(a)–(b)) show that ABC-900 has relative coarse morphology and the amorphous, micropores formed during the activation process. The irregular particles with abundant micropores can provide a large adsorption interface for electrolyte ions, which is beneficial for its EDLC capacitive performance. Fig. 4(d) reveals elemental mapping of the ABC-900 carbon material. The carbon, calcium, phosphorus and silicon elements are uniformly and continuously distributed in it.

To further investigate the electrochemical properties, cyclic

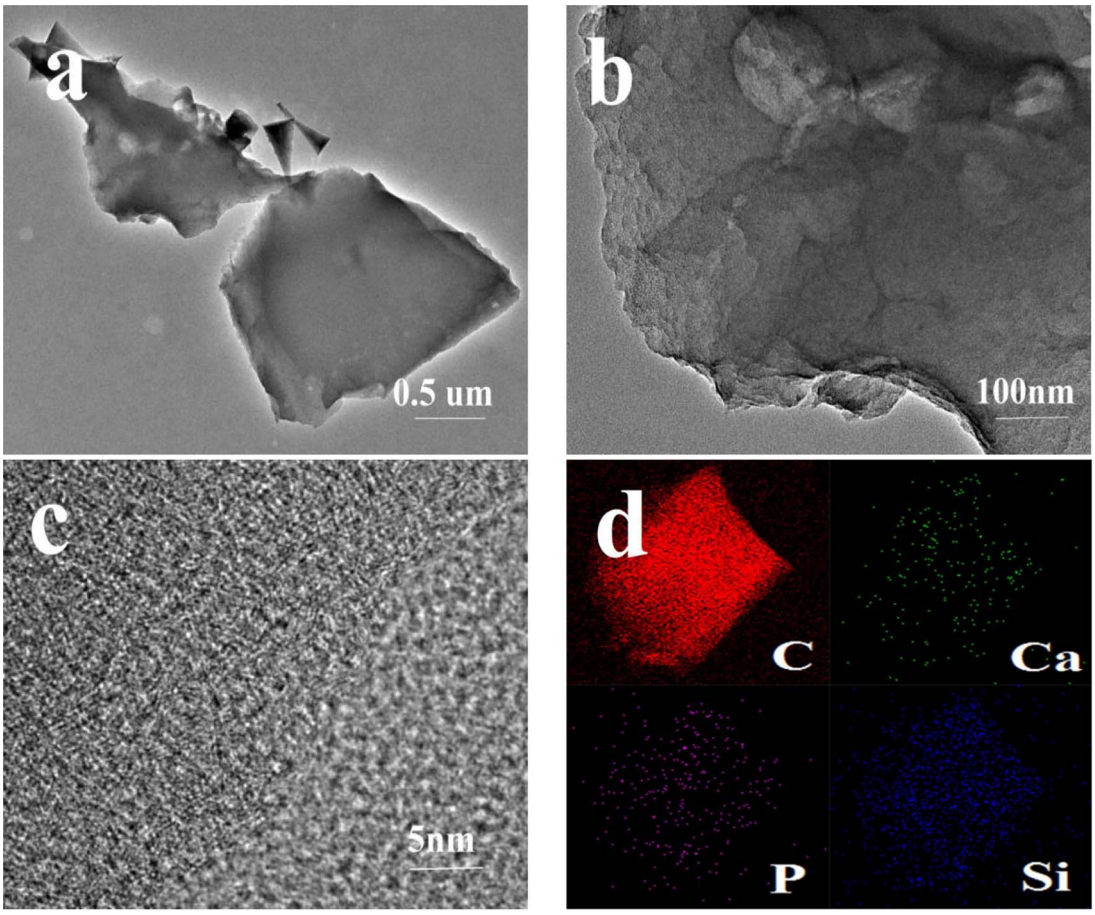

Fig. 4. (a,b) Tem images of ABC-900 carbon material; (c) HRTEM image of ABC-900 carbon material; (d) elemental mapping images of carbon, calcium, phosphorus and silicon elements.

voltammograms (CVs) and galvanostatic charge-discharge measurements (GCDs) are performed in a 3 M KOH aqueous electrolyte. Fig. 5(a) shows the CV curves of the carbon materials at 20 mV s^{-1}. The CV curves show an ideal rectangular-shaped characteristic, typical of electrical double-layer capacitors. The ABC-900 electrode has the largest enclosed area among the electrodes, indicating that the electrode has the highest ability of charge storage. The discharge curves of the carbon materials at 0.5 A g^{-1} are presented in Fig. 5(b). The specific capacitances was calculated according to the following equation [22,23]:

$$C = \frac{I\Delta t}{m\Delta V} \quad (1)$$

where C (unit: F g^{-1}) is the specific capacitance of the carbon electrodes, I is the charge-discharge current, m is the mass of the active electrode, Δt is the charge time (s), and ΔV is the potential charge during the discharge process (V). The specific capacitances calculated from Fig. 4(b) of BC-700, ABC-700, ABC-800, ABC-900 and ABC-1000 are 97.5, 156, 169.2, 293 and 253 F g^{-1} at a current density of 0.5 A g^{-1}, respectively. The specific capacitance of different carbon materials at different current densities are presented in Fig. 5(c). The ABC-900 has a good rate capability (193.8 F g^{-1} even at 20 A g^{-1}), which is much higher than other carbon materials. The high specific capacitance and rate capability should be attributed to the synergistic effect of mesoporous structure and the high BET specific surface area. With the increasing of activation temperature from 700 °C to 900 °C, the pore sizes of the carbon materials decreases, and the ionic nature of electrostatic adsorption increases, resulting in an outstanding capacitance for the activation temperature of 900 °C. In addition, the mesoporous structure can also improve contact at electrode/electrolyte interface, and this further enhances the electrochemical performances of the electrodes. However, the capacitance of ABC-1000 decreases compared with ABC-900, corroborating that only appropriate specific surface areas and pore sizes can improve the electrochemical properties [24].

To further evaluate the electrochemical properties of the carbon materials for practical applications, symmetric supercapacitors device are prepared using the activated carbons in 3 M KOH aqueous electrolyte. The CV curves of the different symmetric supercapacitors at 20 mV s^{-1} are presented in Fig. 6(a). The ABC-900 symmetric supercapacitor has the largest enclosed area, and accordingly the highest ability of charge storage among all the supercapacitors. According to Eq. (1), the specific capacitances of the supercapacitors made of ABC-700, ABC-800, ABC-900, and ABC-1000 electrodes at 0.5 A g^{-1} are 38.3 F g^{-1} (63.8 F cm^{-3}), 43.5 F g^{-1} (72.5 F cm^{-3}), 78.8 F g^{-1} (131.3 F cm^{-3}), and 62.0 F g^{-1} (103.3 F cm^{-3}), respectively, as shown in Fig. 6(b). For other current densities, the specific capacitances of the symmetric supercapacitors are presented in Fig. 6(c). The ABC-900 has a good rate capability (64.7 F g^{-1} even at 20 A g^{-1}), which is much higher than other symmetric supercapacitors.

The electrochemical impedance spectroscopy (EIS) is well-developed to evaluate an electrode's properties such as conductivity, charge-transfer properties, and diffusion properties [25]. Nyquist plots of the

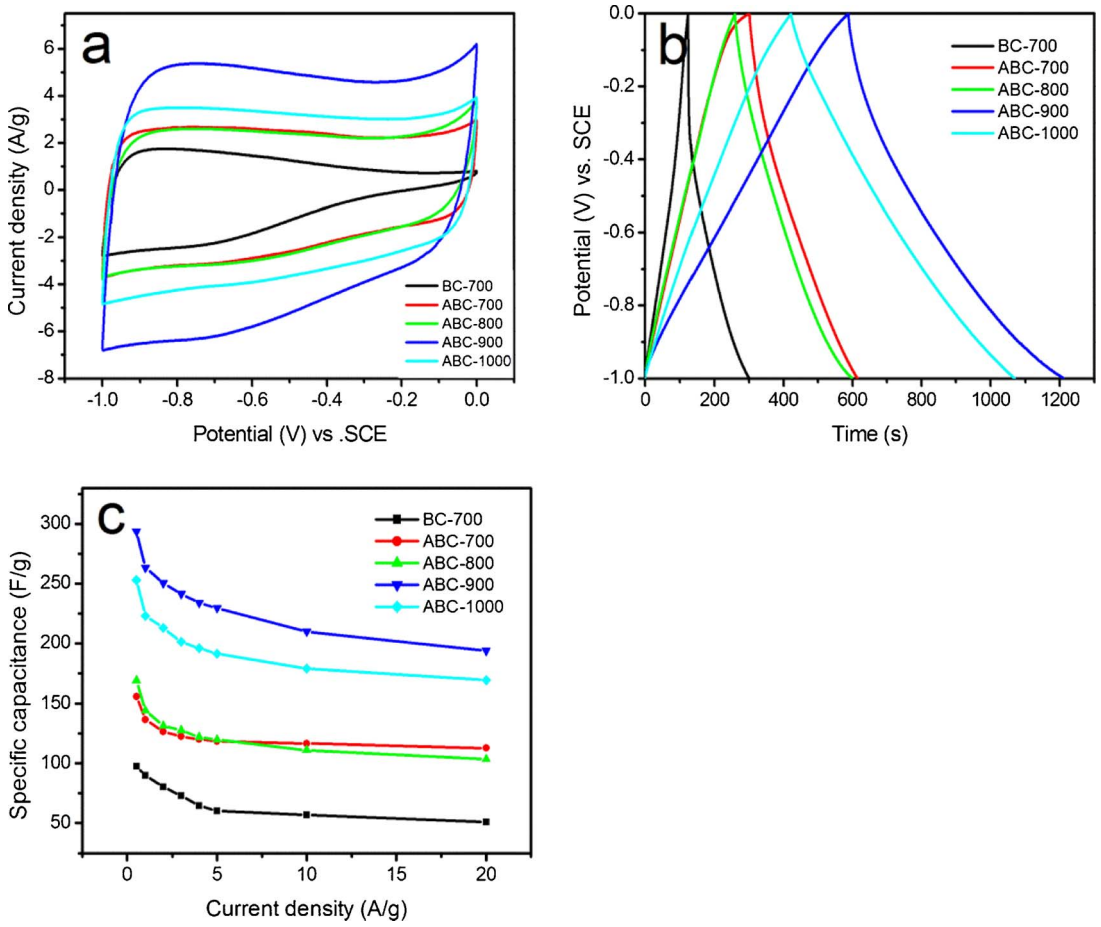

Fig. 5. (a) CV curves scanned at 20 mV s^{-1}; (b) discharge curves at 0.5 A g^{-1}; (c) specific capacitance of the carbon materials at different current densities.

carbon materials in frequencies from 10^5 to 10^{-2} Hz are shown in Fig. 6(d). In the low-frequency region, the straight-line part of the ABC-900 leans more toward the imaginary axis than other carbon materials, indicating that this electrode has a better capacitive behavior. Besides, the Warburg resistance (Z_w) section (a straight line inclined at about 45° to the real axis) is short, illustrating a short diffusion pathway and efficient access of the electrolyte ions to the electrode. The components of the internal resistance (R_S) include the resistance of the electrolyte, intrinsic resistance of substrate, and contact resistance. According to the curves, the values of R_S for ABC-700, ABC-800, ABC-900, and ABC-1000 are 3.6 Ω, 4.8 Ω, 2.2 Ω, and 5.4 Ω, respectively, which are generally low and indicate that the carbon materials have high electrode conductivity. The equivalent circuit used to fit the impedance spectra of the electrode is shown in the inset of Fig. 6d. In the high-frequency region, the diameter of the semicircle represents charge transfer resistance (R_{ct}) in electrochemistry. The semicircular arc of ABC-900 is the smallest among all the carbon materials, and this implies that ion transport in ABC-900 should be the easiest and fastest.

The long-term cycling stability of the symmetric supercapacitors are also measured at 3 A g^{-1}. As shown in Fig. 6(e), the retention rates over 10,000 cycles of ABC-700, ABC-800, ABC-900, and ABC-1000 are 78.1%, 92.1%, 91.8%, and 82.7%, respectively. The high cycling performance of ABC-900 also composes its outstanding electrochemical properties. Energy and power densities for different carbon materials under at different current densities are presented in Fig. 6(f). The energy density (E, Wh kg^{-1}) and power density (P, W kg^{-1}) can been calculated using the following formula [4,22,26]:

$$E = \frac{1}{2}C\Delta V^2 \quad P = \frac{E}{\Delta t}$$

where C (unit: F g^{-1}) is the specific capacitance, ΔV is the potential charge during the discharge process (V), and $\Delta t$is the charge time (s). The symmetric supercapacitor of ABC-900 delivers a high energy density of 10.9 Wh kg^{-1} (18.2 Wh L^{-1}) at a power density of 63 W kg^{-1} (105 W L^{-1}), larger than other supercapacitors in the present study. The value is also higher than those reported in the literature for other carbon materials, such as tobacco rods-derived carbon (8.1 Wh kg^{-1} at 110 W kg^{-1}) [26], fir sawdust-produced carbon fibers (8.4 Wh kg^{-1} at 250 W kg^{-1}) [27], Ultra-small vanadium nitride quantum dots embedded in porous carbon (VNQDs/PC) (10.2 Wh kg^{-1} at 260 W kg^{-1}) [28]. The above comparisons show that the ABC-900 is among the best carbon electrode materials for supercapacitors. Fig. 6(g) shows luminescence of a light-emitting diode (LED) powered by the symmetric supercapacitor with ABC-900 electrodes. This prototype device is able to power the red LED for about 3 min after being fully charged.

4. Conclusions

In summary, activated biomass carbon has been successfully prepared by a simple method involving carbonization and activation processes. For the optimal activation temperature (900 °C), the ABC-900 shows a high surface area (2221.1 $m^2 g^{-1}$), a large capacitance (293 F g^{-1} at a current density of 0.5 A g^{-1}), and an excellent rate

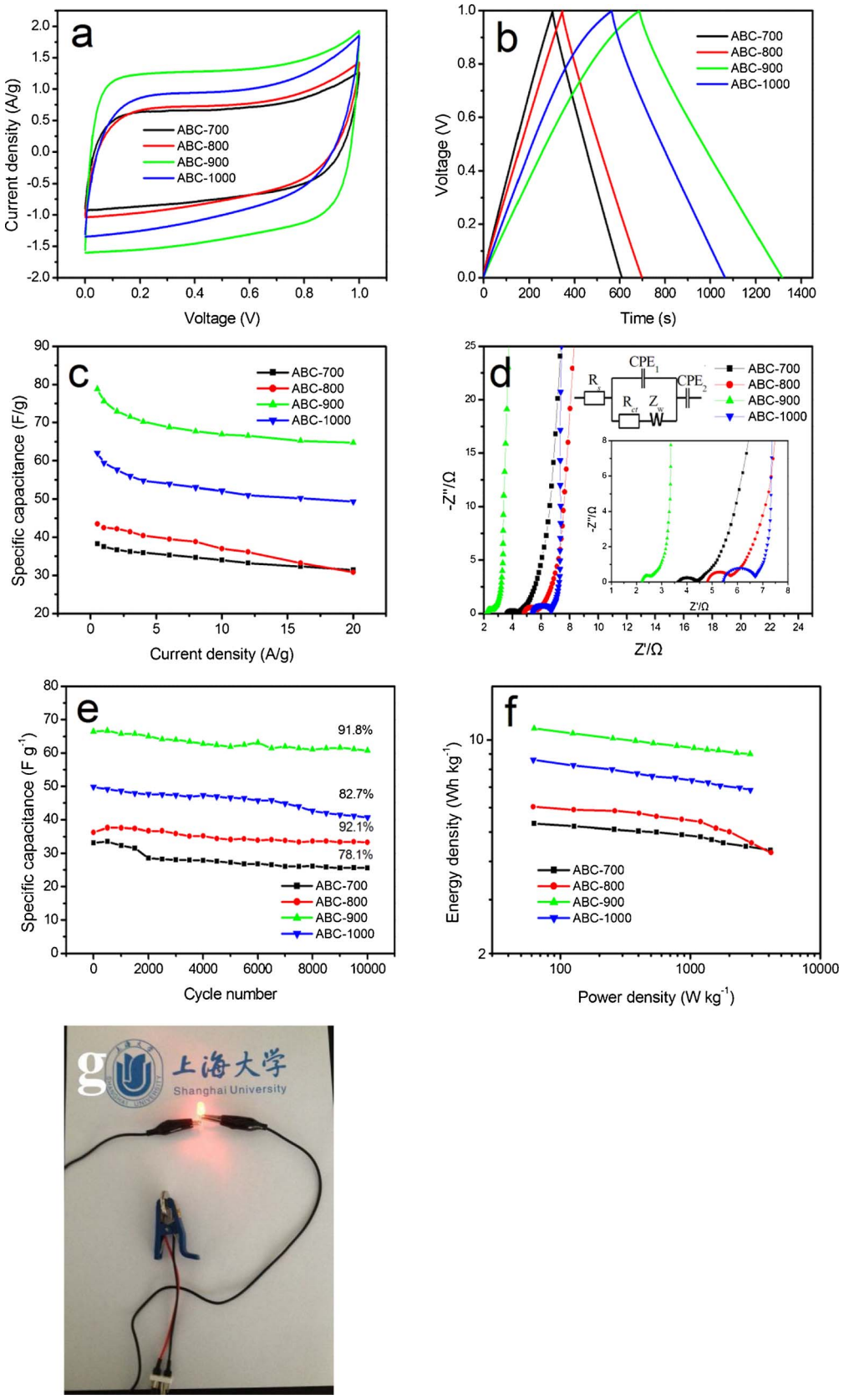

Fig. 6. Electrochemical evaluation of the activated carbon symmetric supercapacitor device: (a) CV curves of different carbon materials at 20 mV s^{-1}; (b) discharge curves of different carbon materials at 0.5 A g^{-1}; (c) The specific capacitance of different carbon materials at different current densities; (d) EIS of different carbon materials; (e) cycling performances of different carbon materials at a current density of 3 A g^{-1}; (f) Energy and power densities for different carbon materials under at different current densities. (g) a LED powered by an symmetric supercapacitor.

capability (193.8 F g^{-1} at a current density of 20 A g^{-1}). The symmetric supercapacitor made of ABC-900 delivers a high energy density of 10.9 Wh kg^{-1} (18.2 Wh L^{-1}) at a power density of 63 W kg^{-1} (105 W L^{-1}) in aqueous electrolytes, and 91.8% retention rate over 10,000 cycles. The excellent performance is attributed to the mesoporous structure that is favorable for transport of ions and electrical contact. These encouraging results show the activated biomass carbon materials are promising for applications in supercapacitors.

Acknowledgements

The work is primarily supported by Shanghai Eastern-scholar program and Shanghai Pujiang Program, China.

References

[1] L.Q. Li, Z.Y. Dai, Y.F. Zhang, J. Yang, W. Huang, X.C. Dong, Carbon@$NiCo_2S_4$ nanorods: an excellent electrode material for supercapacitors, RSC Adv. 5 (2015) 83408–83414.
[2] C.Z. Yuan, H.B. Wu, Y. Xie, X.W. Lou, Mixed transition-metal oxides: design, synthesis, and energy-related applications, Angew. Chem. Int. Ed. 53 (2014) 1488–1504.
[3] J.C. Chen, Y.Q. Liu, W.J. Li, L.Q. Xu, H. Yang, C.M. Li, Nitrogen-enriched carbon sheets derived from egg white by using expanded perlite template and its high-performance supercapacitors, Nanotechnology 26 (2015).
[4] Y. Zhang, X.J. Li, J.F. Huang, W. Xing, Z.F. Yan, Functionalization of petroleum coke-derived carbon for synergistically enhanced capacitive performance, Nanoscale Res. Lett. 11 (2016).
[5] P. Simon, Y. Gogotsi, Materials for electrochemical capacitors, Nat Mater. 7 (2008) 845–854.
[6] Y.T. Luan, L. Wang, S.E. Guo, B.J. Jiang, D.D. Zhao, H.J. Yan, C.G. Tian, H.G. Fu, A hierarchical porous carbon material from a loofah sponge network for high performance supercapacitors, RSC Adv. 5 (2015) 42430–42437.
[7] P. Guillemet, Y. Scudeller, T. Brousse, Multi-level reduced-order thermal modeling of electrochemical capacitors, J. Power Sources 157 (2006) 630–640.
[8] L.L. Zhang, X.S. Zhao, Carbon-based materials as supercapacitor electrodes, Chem. Soc. Rev. 38 (2009) 2520–2531.
[9] K. Kume, N. Kawasaki, H. Wang, T. Yamada, H. Yoshikawa, K. Awaga, Enhanced capacitor effects in polyoxometalate/graphene nanohybrid materials: a synergetic approach to high performance energy storage, J. Mater. Chem. A 2 (2014) 3801–3807.
[10] R. Genc, M.O. Alas, E. Harputlu, S. Repp, N. Kremer, M. Castellano, S.G. Colak, K. Ocakoglu, E. Erdem, High-capacitance hybrid supercapacitor based on multi-colored fluorescent carbon-dots, Sci. Rep. 7 (2017) 13.
[11] S. Repp, E. Harputlu, S. Gurgen, M. Castellano, N. Kremer, N. Pompe, J. Worner, A. Hoffmann, R. Thomann, F.M. Emen, S. Weber, K. Ocakoglu, E. Erdem, Synergetic effects of Fe3+ doped spinel Li4Ti5O12 nanoparticles on reduced graphene oxide for high surface electrode hybrid supercapacitors, Nanoscale 10 (2018) 1877–1884.
[12] S. Kumagai, M. Sato, D. Tashima, Electrical double-layer capacitance of micro- and mesoporous activated carbon prepared from rice husk and beet sugar, Electrochim. Acta 114 (2013) 617–626.
[13] D. Bhattacharjya, J.S. Yu, Activated carbon made from cow dung as electrode material for electrochemical double layer capacitor, J. Power Sources 262 (2014) 224–231.
[14] H. Jin, X. Wang, Y. Shen, Z. Gu, A high-performance carbon derived from corn stover via microwave and slow pyrolysis for supercapacitors, J. Anal. Appl. Pyrol. 110 (2014) 18–23.
[15] E. Redondo, J. Carretero-Gonzalez, E. Goikolea, J. Segalini, R. Mysyk, Effect of pore texture on performance of activated carbon supercapacitor electrodes derived from olive pits, Electrochim. Acta 160 (2015) 178–184.
[16] X. Zhang, Y. Zhao, C. Xu, Surfactant dependent self-organization of Co_3O_4 nanowires on Ni foam for high performance supercapacitors: from nanowire microspheres to nanowire paddy fields, Nanoscale 6 (2014) 3638–3646.
[17] H.C. Chen, J.J. Jiang, L. Zhang, T. Qi, D.D. Xia, H.Z. Wan, Facilely synthesized porous $NiCo_2O_4$ flowerlike nanostructure for high-rate supercapacitors, J Power Sources 248 (2014) 28–36.
[18] G. Yu, L. Lei, J. Yuming, W. Yu, Y. Chuanjun, W. Yingjin, C. Gang, G. Junjie, L. Haiyan, Porous carbon made from rice husk as electrode material for electrochemical double layer capacitor, Appl. Energy 153 (2015) 41–47.
[19] W.H. He, L.H. Lu, Revisiting the structure of graphene oxide for preparing new-style graphene-based ultraviolet absorbers, Adv. Funct. Mater. 22 (2012) 2542–2549.
[20] P. Delhaes, M. Couzi, M. Trinquecoste, J. Dentzer, H. Hamidou, C. Vix-Guterl, A comparison between Raman spectroscopy and surface characterizations of multi-wall carbon nanotubes, Carbon 44 (2006) 3005–3013.
[21] K.R. Ray, R.L. McCreery, Characterization of the surface carbonyl and hydroxyl coverage on glassy carbon electrodes using Raman spectroscopy, J. Electroanal. Chem. 469 (1999) 150–158.
[22] S. Faraji, F.N. Ani, The development supercapacitor from activated carbon by electroless plating—a review, Renew. Sust. Energy Rev. 42 (2015) 823–834.
[23] L.Q. Mai, A. Minhas-Khan, X.C. Tian, K.M. Hercule, Y.L. Zhao, X. Lin, X. Xu, Synergistic interaction between redox-active electrolyte and binder-free functionalized carbon for ultrahigh supercapacitor performance, Nat. Commun. 4 (2013).
[24] J. Chmiola, G. Yushin, Y. Gogotsi, C. Portet, P. Simon, P.L. Taberna, Anomalous increase in carbon capacitance at pore sizes less than 1 nanometer, Science 313 (2006) 1760–1763.
[25] M.-S. Wu, M.-J. Wang, J.-J. Jow, Fabrication of porous nickel oxide film with open macropores by electrophoresis and electrodeposition for electrochemical capacitors, J. Power Sources. 195 (2010) 3950–3955.
[26] Y.Q. Zhao, M. Lu, P.Y. Tao, Y.J. Zhang, X.T. Gong, Z. Yang, G.Q. Zhang, H.L. Li, Hierarchically porous and heteroatom doped carbon derived from tobacco rods for supercapacitors, J. Power Sources 307 (2016) 391–400.
[27] Y.X. Huang, Y. Liu, G.J. Zhao, J.Y. Chen, Sustainable activated carbon fiber from sawdust by reactivation for high-performance supercapacitors, J. Mater. Sci. 52 (2017) 478–488.
[28] Y.L. Yang, L. Zhao, K.W. Shen, Y. Liu, X.N. Zhao, Y.G. Wu, Y.Q. Wang, F. Ran, Ultrasmall vanadium nitride quantum dots embedded in porous carbon as high performance electrode materials for capacitive energy storage, J. Power Sources 333 (2016) 61–71.